

# Ground penetrating radar prototype based on a low-cost software defined radio platform

**Abstract.** Utilizing the software-defined radio (SDR) technique is very common for developing ground penetrating radar (GPR) prototypes. A low-cost SDRs neither allow phase difference estimation between transmitter (Tx) and receiver (Rx). Consequently, direct exploitation of cheap SDRs for GPR is inaccessible. In the paper, an additional calibration step is taken in order to avoid phase difference measurement. The obtained imaging confirms that construction of a simple low-cost subsurface radar is feasible on the basis of the proposed approach.

**Streszczenie.** Wykorzystanie radia programowalnego (SDR – ang. Software Defined Radio) do prototypowania radarów penetracji gruntu (GPR – ang. Ground Penetrating Radar) jest bardzo powszechne. W tanich platformach SDR różnica fazy pomiędzy torem nadawczym i odbiorczym nie jest znana. Dlatego bezpośrednie zastosowanie tanich SDR do GPR jest niemożliwe. W artykule zastosowano dodatkowy krok kalibracyjny w celu uniknięcia pomiaru różnicy faz. Otrzymane zobrażenia potwierdzają możliwość konstrukcji taniego radaru do sondowań podpowierzchniowych. (Prototyp radaru penetracji gruntu bazujący na taniej platformie radia programowalnego)

**Keywords:** GPR, SDR, SFCW, HackRF  
**Słowa kluczowe:** GPR, SDR, SFCW, HackRF

## Introduction

GPR is widely used for recognition of internal structure of different materials. The fundamental principle of that device includes sending the electromagnetic waves into the subsurface and analysing the response from scattering heterogeneities. The intelligible imaging should be the final product of this procedure. A decent interpretation is attainable only after appropriate processing due to the complexity of the environment and the strong influence of the coupling effect.

Besides the computational electromagnetics simulations, hardware testing is a very valuable method for modern processing techniques verifying. Closed architecture and the high cost of commercial devices cause growth in GPR prototyping. Among various approaches [1,2], the SDR is increasingly adopted because of its flexibility and accessibility. Ettus Research is one of the most popular SDR suppliers and offers Universal Software Radio Peripheral (USRP) platforms. Nevertheless, the price of a frequently used platform [3,4] - USRP x310 with two UBX160 cards remains at USD 7872 [5]. The example of using the cheapest USRP (1216 USD) as the GPR can be found in [6].

The article concentrates on building a low-cost stepped frequency continuous wave (SFCW) GPR, in the sense that the total spending should be less than a few hundred USD.

## SDR selection

There are several SDR transceivers available on the market which fulfil GPR condition concerning the wide frequency range. The selected parameters of popular cheap off-the-shelf SDRs are shown in table 1. It is noticeable, solely based on the price, that HackRF is a good proposal for further research.

Table 1. The comparison of selected cheap SDRs parameters [5,7,8]

	USRP B210	BladeRF x40	HackRF
Price [USD]	1216	420	99
Bandwidth [MHz]	30/56	40	20
Freq. range [MHz]	70 - 6000	350 - 3800	1 - 6000
DAC/ADC res. [bit]	12	12	8
Tx max. power [dBm]	10	6	15
Mode	2 x duplex	duplex	half-duplex

HackRF is a completely open source so that some manufacturers offer prices less than 100 USD. The spectrum coverage and maximum transmitter power is sufficient for most of GPR applications, however, performing full-duplex operation requires the second HackRF. The purchase of two such devices is still the cheapest solution, at present.

## Probing signal

Despite applying different ultrawideband (UWB) methods in GPR systems, the SFCW technique is adopted because of its low hardware requirements [9]. Although the operation rate is slower than the speed of other UWB methods, SFCW has several important assets. First of all, it takes advantage of less expensive narrow instantaneous bandwidth devices, because UWB pulse is decomposed into  $K$  individual frequency tones. Moreover, the smaller receiver bandwidth results in improvement of noise figure and dynamic range. Usually, sinusoidal signals are transmitted and received with a uniform frequency step  $\Delta f$  and constant pulse repetition interval  $\Delta t$ , as shown in Fig. 1.

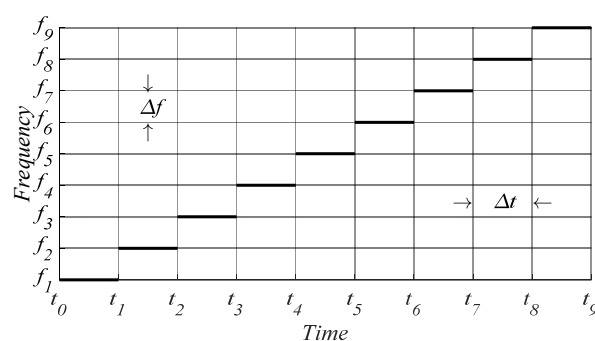


Fig.1. A model SFCW pulse synthesized by  $K=9$  frequency tones

The total bandwidth of this signal is  $B = K\Delta f$ . For each  $k = 1, 2, \dots, K$  frequency, scatter's responses are measured since distance information is related to phase shift. Demodulated baseband IQ signal received in  $k$ -th step is given by:

$$(1) \quad S_k = I_k + jQ_k = A_k \exp(-j\phi_k)$$

where:  $A$  – magnitude,  $\phi$  – phase.

For a sequence of constituent gathered signals a complex vector  $\mathbf{S}$  is obtained.

$$(2) \quad \mathbf{S} = [S_1, S_2, \dots, S_K]$$

Thereafter synthetic range profile  $y_n$  is generated by conversion into the time domain using inverse discrete Fourier transform (IDFT).

$$(3) \quad y_n = \frac{1}{N} \sum_{k=1}^N S_k \exp\left(\frac{j2\pi(n-1)(k-1)}{N}\right)$$

That 1D GPR trace collected in the one point above the surface is called A-scan. In order to produce 2D imaging (B-scan), a set of traces along a specific direction is required.

### Proposed configuration

Most off-the-shelf SDRs produce the same carrier frequency for Tx and Rx, but achieving the phase coherence is a feature of the most expensive SDRs. However, it is usually possible to share the same synchronization clock for Tx and Rx, but after locking ( $t > t_l$ ), phase-locked loops (PLLs) work with unspecified relative phase  $\phi_{rel}$ .

$$(4) \quad \phi_{rel, t > t_l} = \phi_{Tx, t > t_l} - \phi_{Rx, t > t_l}$$

In figure 2 proposed configuration of low-cost GPR is shown. The bistatic radar system is based on two mutually synchronized HackRFs and two antipodal Vivaldi antennas [10].

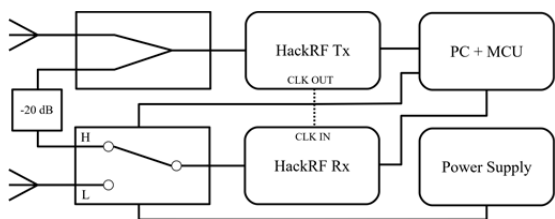


Fig.2. Proposed low-cost GPR on SDR configuration

HackRF Tx is permanently connected through the divider to the Tx antenna. In order to counteract the non-deterministic relative phase, an additional RF switch is used [11]. In the low logical state, a signal from the Rx antenna is connected to HackRF Rx. Otherwise, HackRF Tx and HackRF Rx are coupled through the divider. Supplementary attenuator prevents unintentional damage to the receiver. The switch is triggered by a microcontroller unit (MCU) and powered by the external power supply. The HackRFs and MCU are connected to the PC.

The proposed measurement procedure works on assumption that the switch and internal transmission lines have fixed parameters over the required frequency range and the system is focused only on the analysis of the transmission coefficient between antennas' ports.

For each frequency step, HackRF Rx is fed both by reference Tx signal at a high logic state (H) and the signal from Rx antenna at a low logic state (L). Basically, H and L intervals are not equal due to different delays such as settling time of switch ( $t_s$ ), frequency transition time ( $t_f$ ) and other latencies related to communication and host processing. In order to mitigate the negative impact of that inequalities, triggering binary signal with period  $2\Delta t$  is delayed with respect to the frequency vector. Taking that into consideration, within the  $k$ -th frequency step, a reference signal is collected for a period  $T_{Hk}$  and received signal for a period  $T_{Lk}$  (figure 3). According to this on each

second frequency step, one of the complex numbers ( $S_{Lk}$  or  $S_{Hk}$ ) is estimated more precisely because of longer acquisition. The entire set of recorded results is expressed by vectors:

$$(5) \quad \mathbf{S}_S = [S_{S1}, S_{S2}, \dots, S_{SK}]$$

where:  $K$  – the number of frequency steps,  $S$  – stands for  $L$  or  $H$  and

$$(6) \quad S_{Sk} = I_{Sk} + jQ_{Sk} = A_{Sk} \exp(-j\phi_{Sk})$$

is a  $k$ -th component of  $\mathbf{S}_S$  vector.

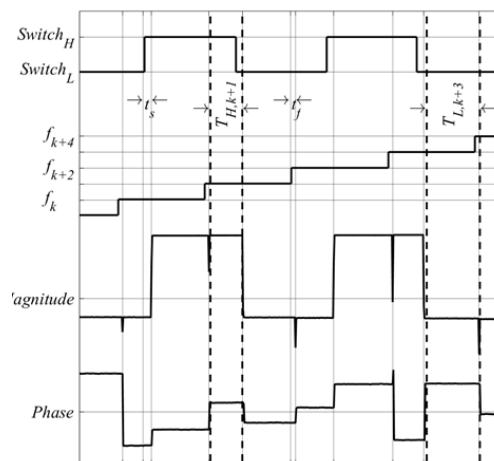


Fig.3. Inequalities of measurement windows

GPR trace is achieved using IDFT of  $\mathbf{S}_{LH}$  vector, the components of which are defined by:

$$(7) \quad S_{LHk} = \frac{S_{Lk}}{S_{Hk}}$$

### Software

GNU Radio Companion (GRC) is very common, multi-platform, and first of all free and open source collection of software radio tools [12], so it has been chosen to build an application for hardware controlling. In figure 4 a flowchart of the transmission part is shown.

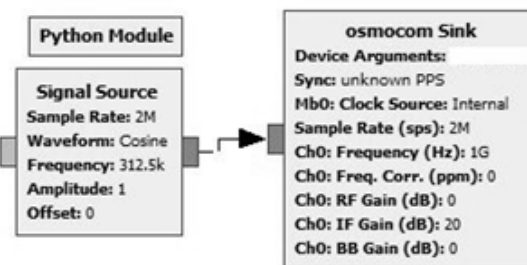


Fig.4. The flowchart of the transmitter

The sink block is simply connected with a cosine signal source. In order to correct Tx power, functions in Python module block correct Tx VGA gain according to the frequency.

HackRF Rx is controlled by a source block (figure 5), and in order to collect individual term of discrete Fourier transform (DFT), Goertzel algorithm is used. It should be pointed out that the sampling rate, length of DFT and selected frequency should be in appropriate relationship to accurately calculate single frequency response.

Diagram responsible for frequency set generation is shown in figure 6. Carrier frequencies for Tx and Rx are evenly spaced over specified interval value and sent at the same time.

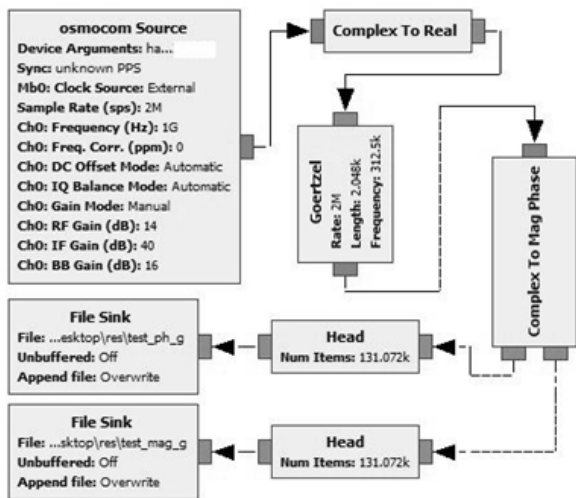


Fig.5. The flowchart of the receiver

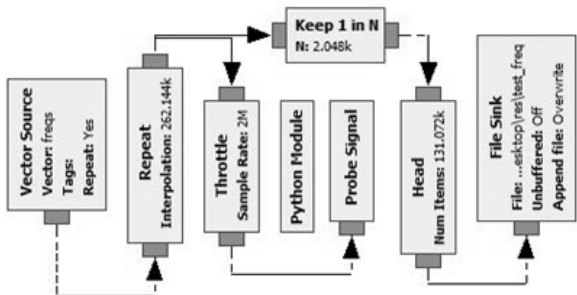


Fig.6. The flowchart of the SFCW sequence generator

RF switch is controlled by STM32 MCU programmed with .NET Micro Framework for communicating with GRC embedded Python block via the serial port. The flowchart of this subsystem is shown in figure 7.

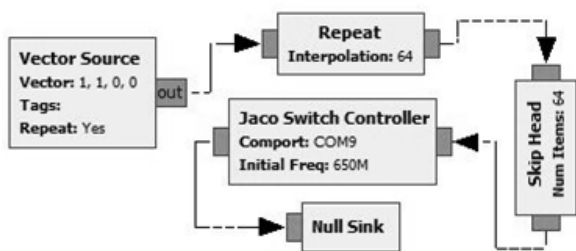


Fig.7. RF switch controller

Recorded data is stored in files which are overwritten for each A-scan. The further analysis consists in cutting specific frames of signal (figure 3) and optional processing prior to or after IDFT calculation.

### Measurement

The prototype system has been tested for capability to create 2D GPR image. The measurement scenario is shown in figure 8. A plastic container with dimensions of approximately 56 x 40 x 28 cm was partially filled with beech wood chips (average chip dimension about 1.5 x 0.7 x 0.5 cm). In general, the relative permittivity of different

woods is  $\epsilon_r = 1.5-3.0$  [13]). The 5 x 5 x 5 cm cubic target was made out of 98% sand ( $\epsilon_r = 2-6$  for dry and  $\epsilon_r = 10-30$  for saturated[14]) and 2% polydimethylsiloxane ( $\epsilon_r = 2.7-2.9$  [15]).

The measurement was conducted three times: without a target, with dry sand cube placed at 8 cm depth and wet target buried 20 cm below surface (10 ml of tap water per 1 cm<sup>3</sup>). GPR traces were collected along x-direction with 1 cm step.

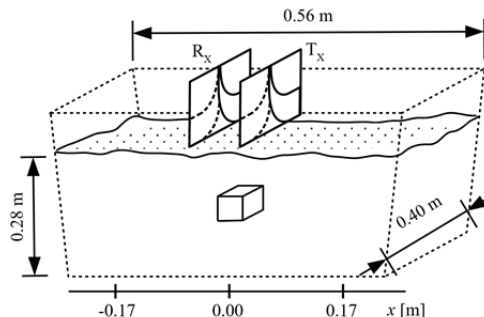


Fig.8. Measurement scenario

The sensor set with the centre-point between antennas was moved 35 times, from  $x = -17$  cm to  $x = 17$  cm. The start frequency was  $f_i = 850$  MHz,  $K = 976$  steps, and  $f_{976} = 5000$  MHz, what gives frequency step  $\Delta f = 4.252$  MHz and  $B = 4150$  MHz. The baseband signal was 312.5 kHz tone in order to prevent overlap with DC component caused by direct-conversion receiver architecture.

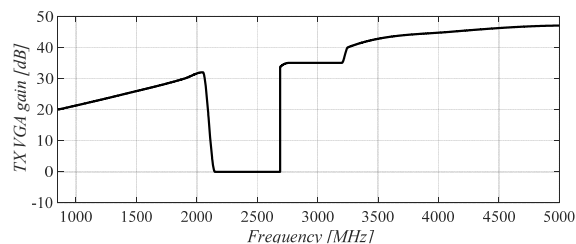


Fig.9. Tx power frequency gain versus operating frequency

HackRF's Tx power varies by operating frequency so that power in whole frequency be similar, a special correction shown in figure 9 was employed.

### Results

The results of the mentioned measurement scenario are shown in figure 10. The presence of darker areas close to  $x = -17$  cm and  $x = 17$  cm is related to the sides of the container and remains similar for each B-scan.

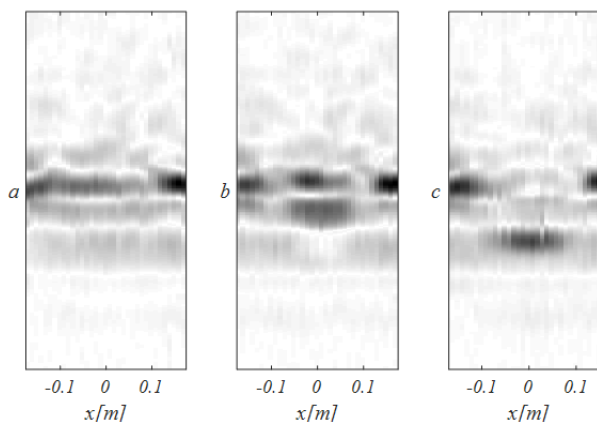


Fig.10. 2D results: a) without a target, b) dry sand cube at a depth of 6 cm, c) wet sand cube at a depth of 20 cm

It is noticeable that the target with higher relative permittivity gives a stronger response. However, shallow buried dry sand with dielectric constant closer to  $\epsilon_r$  of the surrounding medium is distinct either.

The average variance of the measured phase within the each of possible relation between measuring windows –  $T_{Hk}/T_{Lk}$  (figure 3) is shown in figure 11. Generally, even for shorter windows, the variance is less than 0.0002 rad.

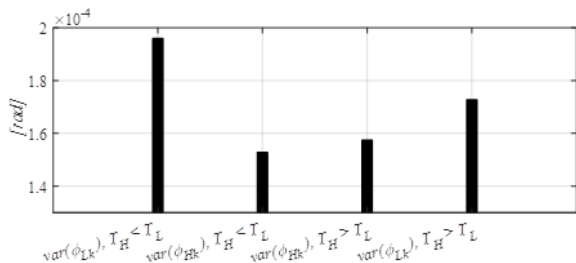


Fig.11. Average variance of phase within each possible measuring window

There is a slight growth of fluctuation in the signal phase from the Rx antenna ( $\phi_L$ ), mainly related to external interference.

### Conclusion

These results demonstrate that GPR prototype based on low-cost SDR is achievable. Suggested configuration and calibration enable real data gathering and permit interpretable imaging of simple subsurface structures to be produced. The described approach will allow researchers without access to expensive devices a rapid introductory analysis of implemented GPR or other remote sensing signal processing algorithms.

**Authors:** prof. dr hab. inż. Mateusz Pasternak, Wydział Elektroniki, Wojskowa Akademia Techniczna, ul. Gen. Witolda Urbanowicza 2, 00-908 Warszawa 46, E-mail: [mateusz.pasternak@wat.edu.pl](mailto:mateusz.pasternak@wat.edu.pl); mgr inż. Jacek Jendo, Wydział Elektroniki, Wojskowa Akademia Techniczna, ul. Gen. Witolda Urbanowicza 2, 00-908 Warszawa 46, E-mail: [jacek.jendo@wat.edu.pl](mailto:jacek.jendo@wat.edu.pl).

### REFERENCES

- [1] Pasternak M. et al., Stepped frequency continuous wave GPR unit for unexploded ordnance and improvised explosive device detection, *2011 12th International Radar Symposium (IRS)*, 105-109
- [2] Ferrara V. et al., Design and realization of a cheap ground penetrating radar prototype @ 2.45 GHz, *2016 10th European Conference on Antennas and Propagation (EuCAP)*, 1-4
- [3] Carey S.C., Scott W. R., Software defined radio for stepped-frequency, ground-penetrating radar, *2017 IEEE International Geoscience and Remote Sensing Symposium (IGARSS)*, 4825-4828
- [4] Jenks C. H. J., Pennock S. R., The use of a software defined radio as an OFDM GPR, *2017 9th International Workshop on Advanced Ground Penetrating Radar (IWAGPR)*, 1-4
- [5] <https://www.ettus.com>, January 2019
- [6] Colorado J. et al., An integrated aerial system for landmine detection: SDR-based Ground Penetrating Radar onboard an autonomous drone, *Advanced Robotics*, 31:15, 791-808, 2017
- [7] <https://www.nuand.com>, January 2019
- [8] <https://pl.aliexpress.com/store/2957122>, January 2019
- [9] Kaczmarek P., Łapiński M., Silko D., Synthetic range profiling in ground penetrating radar, *Proc. SPIE 7502, Photonics Applications in Astronomy, Communications, Industry, and High-Energy Physics Experiments (2009)*
- [10] Pasternak M., Pietrański J., Antysymetryczna antena Vivaldi do zastosowań w radarach penetracji gruntu, *43 Konferencja Naukowo-Techniczna Radiolokacji (2011)*
- [11] Marimuthu J., Białkowski K. S., Abbosh A. M., Software-defined radar for medical imaging, *IEEE Transactions on Microwave Theory and Techniques*, vol. 64 (2016), no. 2, 643-652.
- [12] <https://www.gnuradio.org>, January 2019
- [13] Кочеткова Т. Д., Суслев В. И., Волчков С. И., Диэлектрическая проницаемость хвойных пород древесины в диапазоне частот 3-12 ГГц, *Сибирский журнал науки и технологий*, 51 (2013), №5
- [14] Martínez A., Byrnes A. P., Modeling dielectric-constant values of geologic materials: an aid to ground-penetrating radar data collection and interpretation, *Current Research in Earth Sciences*, Bulletin 247 (2001), part 1
- [15] Cresson P. -. et al., 1 to 220 GHz complex permittivity behavior of flexible polydimethylsiloxane substrate, *IEEE Microwave and Wireless Components Letters*, vol. 24 (2014), no. 4, 278-280